Hindawi
Mathematical Problems in Engineering
Volume 2018, Article ID 4746210, 15 pages
https://doi.org/10.1155/2018/4746210

Research Article

An Improved Sucker Rod Pumping System Model and Swabbing Parameters Optimized Design

Weicheng Li,[1,2] **Shimin Dong**,[1] **and Xiurong Sun**[1]

[1]*School of Mechanical Engineering, Yanshan University, Qinhuangdao, 066004, China*
[2]*School of Engineering, King's College, University of Aberdeen, Aberdeen, AB24 3UE Scotland, UK*

Correspondence should be addressed to Shimin Dong; ysudshm@163.com

Received 28 December 2017; Accepted 15 October 2018; Published 30 October 2018

Academic Editor: Gen Q. Xu

Considering the impact of fluid flowing into pump on sucker rod pumping system (SRPS) dynamic behaviors, an improved SRPS model with new boundary model is presented, which is a fluid-solid coupled model with the interactions among surface transmission, rod string longitudinal vibration, plunger motion, and fluid flow. A uniform algorithm is adopted instead of the mixed iteration algorithm for the surface transmission and downhole rod string vibration submodels, to reduce the difficulties of solving the entire SRPS model. The dynamic response comparison is executed between the improved model and the current model, and the results show that it will bring a calculation error on pump load and pump fullness if the progress of fluid flowing into the pump (PFFP) is ignored. Based on this improved model, a multitarget optimization model is proposed and the dynamic behavior of SRPS is improved with the optimized swabbing parameters.

1. Introduction

The SRPS is widely used in oil fields. It comprises three parts: surface transmission unit converting rotational motion into linear motion, sucker rod string as a joint between surface and downhole, and reciprocating pump exploiting the oil (see Figure 1). The importance of predicting the dynamic responses of SRPS is to determine the operating situation and oil production [1]. For this equipment is usually set up in an open-air environment, and the test data device mounted on it is usually broken, especially the main working subsystem which is located nearly one kilometer or more downhole, making it difficult to be tested. Therefore, a more accurate SRPS simulation model should be established although the research in this field of study has been carried out widely. Due to the slender rod string moving upwards and downwards all time, an intense longitudinal vibration is produced. According to Figure 1, the SRPS model can be divided into rod string longitudinal vibration model, surface transmission model, and downhole pumping model. Commonly, this model is solved using the rod string longitudinal vibration equation as the foundation, surface and downhole model as boundary conditions. The most successful model of rod string longitudinal vibration is the Gibbs's wave equation, and based on that, the models are studied specifically on the enhancement of the surface and downhole boundaries with different operating conditions [2–4]. The surface boundary condition that includes the motor speed variations has been extensively used and is more applicable in practice [5, 6] whereas the downhole boundary condition has been continuously improved. However, further study is still required due to the inconsistent alteration and complication encountered in downhole operation.

The downhole boundary condition actually is a model describing the pump operation. The pump operating mode can be divided into upstroke and downstroke. During upstroke, as the plunger moves upwards, the pump pressure will decrease and the fluid will not be sucked into the pump until this pressure drop down to pump inlet pressure. For the downstroke, the pressure will increase with the plunger goes down and the fluid will begin to be drained out when the pressure equals the pump outlet pressure. Based on the SRPS's operating state, the first universal downhole boundary model was divided into four phases with a vague formulation

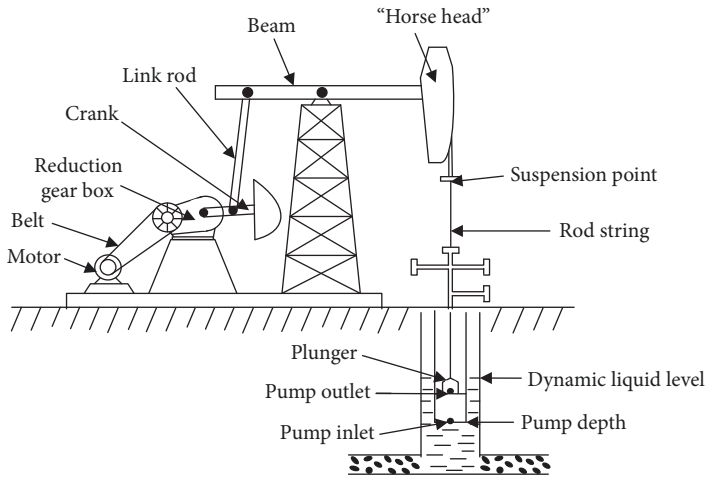

Figure 1: Sucker rod pumping system.

[2]. In an ideal condition, during the fully loaded upstroke movement, the pump load was set equivalent to the fluid load; pump load was set to zero for the unloaded downstroke movement [7, 8]. As the pump operation phases are highly related to pump pressure, it was revised with an explicit formation deduced by the interaction between pump outlet pressure and the pressure in the pump barrel [9–14], as follows:

$$F_{PL}(t) = A_p(p_d - p) - A_r p_d \tag{1}$$

where F_{PL} is the pump load, N; A_p and A_r are the cross section area of plunger and rod string respectively, m^2; p_d is the pump outlet pressure, pa; p is the pump pressure, pa.

For the p_d is always considered as a constant pressure, the key of this research is to establish an accurate pump pressure model which consists of four phases as shown in Figure 2. With considering of the gas, this downhole boundary model is improved as shown in (2). When the pump is at phases 1 and 3, the pressure variation obeys the rules of gas state equation. As for in phases 2 and 4, the pump pressure is taken as the p_s and p_d separately.

$$\begin{aligned}
p &= \left(\frac{L_{og}}{L_{og} + u_p - \int_0^{t_s}(q/A_p)}\right)^Q p_d \quad \text{phase 1} \\
p &= p_s \quad \text{phase 2} \\
p &= \left(\frac{L_g}{L_g - L_s + u_p - \int_{t_u}^{t_t}(q/A_p)}\right)^Q p_s \quad \text{phase 3} \\
p &= p_d \quad \text{phase 4}
\end{aligned} \tag{2}$$

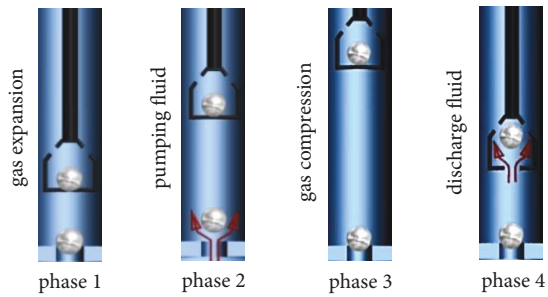

Figure 2: Four phases of pump operation.

where L_{og} and L_g are the gas column length when plunger is arriving at bottom dead center and top dead center, respectively, m; u_p is the plunger displacement, m; L_s is the pump stroke displacement, m; L_p is the plunger length, m; μ is the fluid dynamic viscosity, pa·s; δ is the clearance between plunger and pump barrel, m; D_d is the pump diameter, m; t_s and t_t are the open time of standing valve and travelling valve, respectively, s; t_u is the upstroke time; q is the liquid instantaneous leakage volume.

In this formula, the principle that the gas/oil ratio of clearance volume (the space volume when plunger arrives at bottom dead center) equals the gas/oil ratio of pump inlet is applied. However, at this time, the pump pressure should be the same as the pump outlet pressure. Thus, it is revised with the pump outlet pressure and this improved model has been widely used until now. [15–18]. However, the current downhole boundary model still exists some shortcomings need to be improved. Due to ignoring the progress of PFFP, it is established with the hypothesis of regarding the pump is filled with the fluid, whose gas/liquid ratio always equals that at pump intake, as well as the one in the clearance volume. This assumption is not applicable for the oil well with insufficient oil well deliverability (OWD) which will

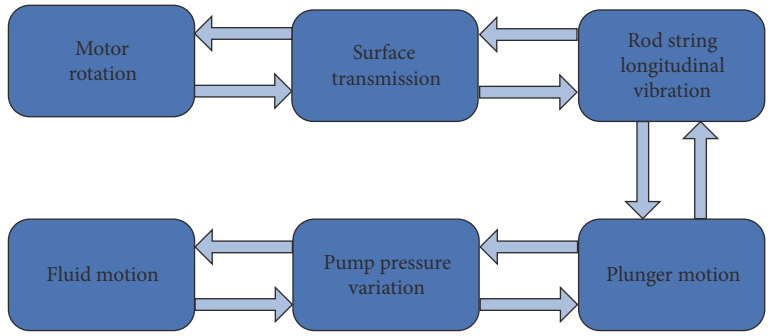

Figure 3: SRPS coupled model sketch.

result in the pumping fluid being unable to keep pace with the plunger and cause an incomplete fullness. Meanwhile, a pump load calculation error will be produced with keeping the pump pressure as constant when fluid flows into the pump.

The SRPS model lays the foundation for optimizing the swabbing parameters to improve the system operation status, except for predicting and evaluating its dynamic response. Miska et al., 1997 [19], propose a computer-aided optimization method relying on a simple linear algebraic system model, so as to minimize the energy consumption. Firu et al., 2003 [20], present an improve optimization criterion including eight operational parameters to achieve the maximum system efficiency. Liu and Qi, 2011 [21], apply fluid flow characteristics in coalbed methane reservoirs to estimate the production capacity and build the system efficiency optimization model combined with SRPS performance. The above optimization models are built with a simplified pump load; then an improved system efficiency optimization model is built jointing with formula (2) [22, 23]. However, the current optimization models ignore the effect of swabbing parameters on pump fullness, in that the SRPS model's restriction. Besides that, single target optimization cannot make an accurate and comprehensive presentation for SRPS whose pumping progress is complex, multicomponent and interactive.

In this paper, firstly, an improved SRPS model is presented with the new downhole boundary model, considering the movement of fluid flowing into pump with gas instantaneous dissolution and evolution. Secondly, for the new downhole boundary model, a nonlinear fluid-solid coupled model will increase the complexity of this improved SRPS model. A unified numerical algorithm is applied on the whole model to decrease the calculation time, instead of traditional mixed iteration algorithm. Thirdly, a multiobjective optimization model is proposed based on the improved SRPS model. Fourthly, the surface dynamometer card is collected to verify the improved model's accuracy. Fifthly, the dynamic response comparison on the current SRPS model and improved SRPS model is executed. Finally, the optimization program is applied on a test well, and the results are given before and after optimization.

2. Integrated Simulation Model

The improved SRPS model is a nonlinear fluid-solid coupled model consisted of drive, transmission and load. The motor is used to generate power and its rotation motion is transformed into linear motion of suspension point. This linear motion is passed on to the plunger through rod string longitudinal vibration; meanwhile, plunger motion has an influence on pumping fluid by regulating pump pressure. On the contrary, fluid motion affects pump pressure which is also the main factor in determining pump load. This pump load and other system loads are transferred to motor output shaft by surface and downhole transmission, causing impact on the motor motion. The above coupled process is depicted in Figure 3. In this paper, the SRPS model is subdivided into rod string longitudinal vibration model, corresponding surface boundary and downhole boundary model, so as to have a clear description.

2.1. Sucker Rod Longitudinal Vibration Model. While the SRPS is operating, the motion of arbitrary micro element of the slender rod string produced intense longitudinal vibration can be composed of the following two parts: (1) following the movement of suspension point and (2) relative movement to the suspension point. Referring to Figure 4, the coordinate system is built based on the top dead center of horse head as the origin. Then the stress balance terms of rod string element and top and bottom boundary conditions are used to establish the sucker rod longitudinal vibration model, with the assumption of ignoring the deformation of tube and the vibration of liquid column in a vertical well.

$$\begin{aligned}
&\frac{\partial^2 u}{\partial t^2} - \frac{E_r}{\rho_r}\frac{\partial^2 u}{\partial x^2} + \frac{\mu}{\rho_r A_r}\frac{\partial u}{\partial t} \\
&\quad = -\frac{d^2 u_a(t)}{dt^2} - \frac{\mu}{\rho_r A_r}\frac{du_a(t)}{dt} + g \\
&u(x,t)|_{x=0} = u_a(t) \\
&E_r A_r \left.\frac{\partial u(x,t)}{\partial x}\right|_{x=L_r} = F_{PL}(t)
\end{aligned} \tag{3}$$

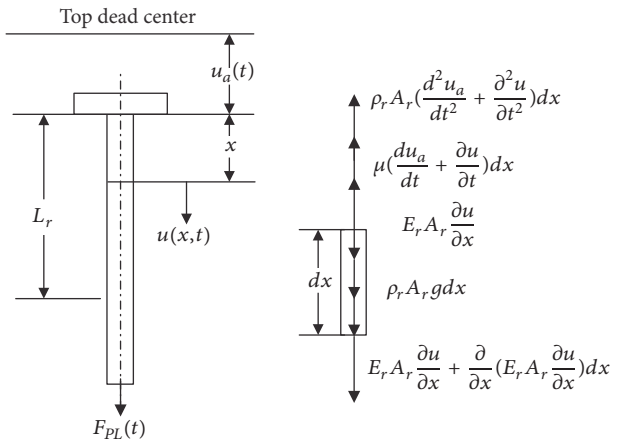

Figure 4: Mechanical model of rod string longitudinal vibration.

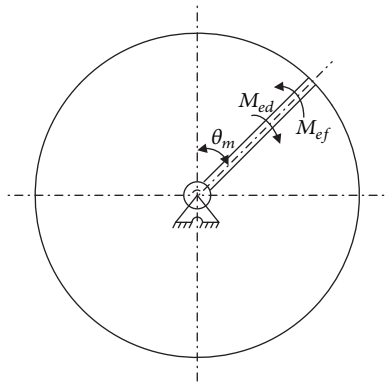

Figure 5: Surface apparatus equivalent motion model.

where u is the displacement of the rod string at arbitrary depth and time, m; E_r and ρ_r are the elasticity modulus and density of rod string, respectively, pa and kg/m^3; u_a is the suspension point displacement, m.

2.2. Surface Boundary Model. The surface boundary condition refers to the motion of suspension point as in (3). With the assumption that the surface transmission mechanism consists of belt-reducing gear and four-bar linkage as a single degree of freedom system, it can be represented as a function of motor angle. Later, the surface apparatus motion model is set up using Lagrange equation, taking motor output shaft as equivalent component, its motion as generalized coordinates and set 12 o'clock as a reference direction (Figure 5).

$$\begin{aligned} I_e\ddot{\theta}_m + \frac{1}{2}\dot{\theta}_m{}^2 \frac{dI_e}{d\theta_m} &= M_{ed} - M_{ef} \\ \theta_m\big|_{t=0} &= 0 \\ \dot{\theta}_m\big|_{\theta=0} &= \omega_0 \end{aligned} \tag{4}$$

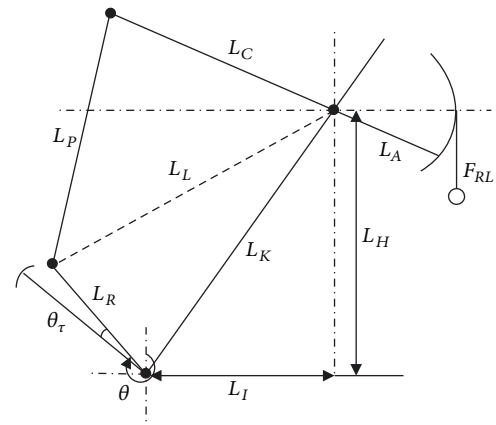

L_R— crank
L_P— link rod
L_C— beam back
L_A— beam front

Figure 6: Four-bar linkage.

With the equivalent rotating inertia

$$I_e = \sum I_j \left(\frac{\omega_j}{\dot{\theta}_m}\right)^2 + \sum m_j \left(\frac{v_j}{\dot{\theta}_m}\right)^2 \tag{5}$$

The semiempirical formulation of motor driving torque M_{ed} deduced from the speed/torque characteristic is adopted from Wu et al. [24].

$$M_{ed} = \frac{2\lambda_k M_H \varepsilon_c \omega_n \left[\omega_n - \dot{\theta}_m\right]}{\varepsilon_c^2 \omega_n^2 + \left[\omega_n - \dot{\theta}_m\right]^2} \tag{6}$$

where λ_k is the motor overload coefficient; ε_c is the motor critical-slip ratio; ω_n is the motor synchronous angular velocity, rad/s.

$$\begin{aligned} M_H &= 9550\frac{P_H}{n_H} \\ \varepsilon_c &= \varepsilon_r\left(\lambda_k + \sqrt{\lambda_k^2 - 1}\right) \\ \omega_n &= \frac{2\pi f}{z} \end{aligned} \tag{7}$$

where z is the motor pole pairs; f is the power frequency, Hz; P_H is the motor rated power, kW; n_H is the motor rated speed, min^{-1}; ε_r is the motor rated-slip ratio.

The equivalent resistance torque is derived in accordance with the force balance of four-bar linkage (Figure 6), written as

$$M_{ef} = \frac{1}{i_{bg}\varepsilon_b}\left[S_{Tf}\left(F_{RL} - F_b\right)\varepsilon_p^{k_1} - M_c \sin\left(\theta - \theta_\tau\right)\right] \tag{8}$$

with the angle of crank

$$\theta = \frac{\theta_m}{i_{bg}} \tag{9}$$

where i_{bg} is the transmission ratio of the belt-reducing gear system; ε_p is the transmission efficiency from crank to suspension point; S_{Tf} is torque factor, m; F_{RL} is the suspension point load, N; F_b is the structural unbalance weight, N; M_c is the maximum balancing torque of the crank N·m.

The displacement of suspension point can be expressed as motor angle, based on the geometry relation shown in Figure 6 [6]. The surface boundary motion model is

$$u_a(t) = \arccos\left[\frac{L_C^2 + L_K^2 - (L_R + L_P)^2}{2L_C L_K}\right] - \arccos\left(\frac{L_C^2 + L_L^2 - L_P^2}{2L_C L_L}\right) - \arcsin\left(\frac{L_R}{L_L} \cdot \sin\left(2\pi - \theta_0 - \frac{\theta_m}{i_{bg}} + \arcsin\left(\frac{L_I}{L_K}\right)\right)\right) \tag{10}$$

2.3. Downhole Boundary Model. This new model is an improved method from the current boundary models considering the interaction among pump pressure, fluid flow into pump, gas dissolution and evolution, pressure drop due to fluid gravitational potential energy, inertia head loss, friction head loss, and local head loss. The new boundary model consists of pressure variation model and fluid flow into pump model. Some assumptions are made for building this model:

(1) Bottom dead point of plunger as the origin position.

(2) The pump inlet pressure p_s and outlet pressure p_d are kept constant for one cycle of SRPS operation.

Pressure Variation Model. The gas state equations are built as follows ((11) and (12)) when the displacement of plunger is u_p or u_p+du_p:

$$p\left[\left(u_p + L_{og} - L_f - L_k\right) A_p\right] = ZNQT \tag{11}$$

$$(p + dp) \cdot \left[\left(u_p + du_p + L_{og} - L_f - L_k - dL_f - dL_k\right) A_p\right] = \left(Z + \frac{\partial Z}{\partial p} dp\right)(N + dN) QT \tag{12}$$

where N is the gas molar number, mol; Q is the natural gas constant, J/(mol·K); T is the temperature in pump barrel, ˚C; Z is the natural gas compressibility factor; L_k is the equivalent length of pump leakage, m; L_f is the liquid level in the pump, m.

Dividing (11) by (12) and ignoring the second order small quantities, then the variation of pump pressure with plunger displacement is obtained:

$$\frac{dp}{du_p} = \frac{(1/N)\left(dN/du_p\right) + \left(1/\left(u_p + L_{og} - L_f - L_k\right)\right)\left(d\left(L_f + L_k\right)/du_p - 1\right)}{p^{-1} - (1/Z)\left(dZ/dp\right)} \tag{13}$$

The above equation is converted into a time varying function with the purpose of facilitating it with the rod string longitudinal vibration equation.

$$\frac{dp}{dt} = \frac{(1/N)\left(dN/dt\right)\left(1/v_p\right) + \left(1/\left(u_p + L_{og} - L_f - L_k\right)\right)\left(\left(d\left(L_f + L_k\right)/dt\right)\left(1/v_p\right) - 1\right)}{p^{-1} - (1/Z)\left(dZ/dp\right)} v_p \tag{14}$$

where v_p is the plunger velocity, m/s.

From (14), dN is composed of the following sections.

(1) The molar number of gas is released from or dissolved into oil as pressure varies

$$dN_r = -\frac{ZTp_{st}}{Z_{st}T_{st}p}(\alpha \cdot dp) \cdot \frac{10^3 A_p\left(L_f + L_o - L_{og}\right)(1 - \varepsilon_w)}{B_o V_{mol}} \tag{15}$$

where p_{st} is the standard pressure, pa; Z_{st} is the standard natural gas compressibility factor; T_{st} is the standard temperature, ˚C; α is the solubility coefficient of natural gas $m^3/(m^3 \cdot pa)$; ε_w is the water content; V_{mol} is the molar volume, m^3; B_o is the crude oil volume factor.

(2) The molar number of gas with fluid being sucked into the pump corresponding to the pump pressure is

$$dN_s = \frac{10^3 A_p R_J dL_f}{V_{mol}} \tag{16}$$

where R_J is the transient gas liquid ratio in the pump, m^3/m^3.

(3) The molar number of gas with leaked fluid at the pump pressure is

$$dN_v = \frac{10^3 A_p R_J dL_v}{V_{mol}} \tag{17}$$

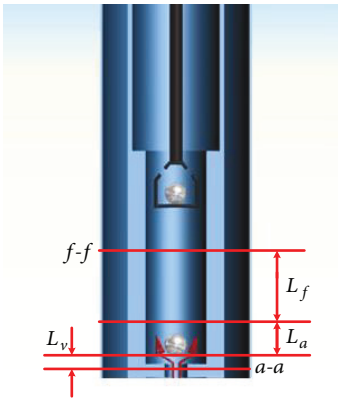

FIGURE 7: Process of fluid flows into the pump.

where

$$R_J = (1 - \varepsilon_w)(R_p - R_s)\frac{p_{st} Z T}{T_{st} Z_{st} p}$$
$$R_s = \alpha (p - p_{st}) \tag{18}$$

where R_p is the production gas oil ratio, m^3/m^3; R_s is the gas oil ratio at pump intake, m^3/m^3.

Fluid Flowing into Pump Model. Figure 7 shows the pump operation when the gas-liquid flow is drawn into the pump. Section *a-a* indicates the cross section of standing valve hole. Supposing the section *f-f* is the liquid level at arbitrary time, neglect the process of gas bubbling from fluid by considering only the pump gas to occupy the upper space of *f-f*. The one-dimensional unsteady flow equation based on Bernoulli equation is established to describe the flow state of pumping liquid. In the Bernoulli equation, the inertia head loss, friction head loss, and local head loss are all considered.

$$\frac{p_s}{\rho g} + \frac{v_a^2}{2g} = \frac{p}{\rho g} + \frac{v_f^2}{2g} + \left(L_o - L_{og} + L_f + L_v\right) + h_a + h_v + h_f \tag{19}$$

where

$$h_a = \frac{1}{g}\left(L_o - L_{og} + L_f + L_v \frac{A_f}{A_p}\right)\frac{dv_f}{dt}$$
$$h_f = \frac{64 \mu v_f \left(L_o - L_{og} + L_f\right)}{2 D_d^2 \rho g}$$
$$h_v = \frac{1}{g\varepsilon^2}\left(\frac{A_p}{A_f}\right)^2 \frac{v_a^2}{2} \tag{20}$$
$$v_a = \frac{A_p}{A_f} v_f$$

where ε is the flow coefficient of standing valve.

Then (19) is converted into differential forms.

$$\dot{L}_f = v_f$$
$$\dot{v}_f = \left(L_0 - \frac{V_{og}}{A_p} + L_f + L_v \frac{A_f}{A_p}\right)^{-1} \left\{\frac{p_s}{\rho} - \frac{p}{\rho} + \frac{v_f^2}{2}\left[\frac{A_p^2}{A_f^2} - \frac{A_p^2}{\varepsilon^2 A_f^2} - \frac{64 \mu \left(L_0 - V_{og}/A_p + L_f\right)}{D_d^2 v_f \rho} - 1\right] - g\left(L_0 - \frac{V_{og}}{A_p} + L_f + L_v\right)\right\} \tag{21}$$

Normally, the fluid in the barrel, no matter in which form, will all be discharged except the one in dead space. Therefore, the fluid flowing out of the model with opening traveling valve is not proposed. The pump outlet pressure generated by several kilometers liquid column is large compared to the hydraulic loss, causing the ignorance of hydraulic loss when fluid flows out. Based on the statement mentioned above, the new downhole boundary model is expressed as follows and also is divided into four phases corresponding to the phases shown in Figure 2:

*Status*1: *before opening the standing valve*

$$\frac{dp}{dt} = \frac{\left(q/\left(A_p \cdot v_p\right)\right)\left(1/\left(u_p - L_v + L_{og}\right) + \left(10^3 A_p \cdot R_J\right)/\left(N \cdot V_{mol}\right)\right) - 1/\left(u_p - L_v + L_{og}\right)}{\left[p^{-1} - 1/Z \cdot dZ/dp + 10^3 \alpha/N \cdot Z T p_{st}/T_{st} p \cdot \left(L_v + L_o - L_{og}\right)/s_p V_{mol} \cdot A_p \cdot (1 - \varepsilon_w)\right]} \cdot v_p$$

*Status*2: after *opening the standing valve*

$$\frac{dp}{dt} = \frac{\left(\left(v_f \cdot A_p + q\right)/\left(A_p \cdot v_p\right)\right)\left(1/\left(u_p - L_f - L_v + L_{og}\right) + \left(10^3 A_p \cdot R_J\right)/\left(N \cdot V_{mol}\right)\right) - 1/\left(u_p - L_f - L_v + L_{og}\right)}{\left[p^{-1} - 1/Z \cdot dZ/dp + 10^3 \alpha/N \cdot Z T p_{st}/T_{st} p \cdot \left(L_v + L_f + L_o - L_{og}\right)/s_p V_{mol} \cdot A_p \cdot (1 - \varepsilon_w)\right]}$$

$$\cdot v_p$$

*Status*3: before *opening the traveling valve*

$$\frac{dp}{dt} = \frac{\left(q/\left(A_p \cdot v_p\right)\right)\left(1/\left(u_p - L_f - L_v + L_{og}\right) + \left(10^3 A_p \cdot R_J\right)/\left(N \cdot V_{mol}\right)\right) - 1/\left(u_p - L_f - L_v + L_{og}\right)}{\left[p^{-1} - 1/Z \cdot dZ/dp + 10^3\alpha/N \cdot ZTp_{st}/T_{st}p \cdot \left(L_v + L_f + L_o - L_{og}\right)/s_p V_{mol} \cdot A_p \cdot \left(1 - \varepsilon_w\right)\right]} \cdot v_p$$

*Status*4: after *opengin the traveling valve*

$$\frac{dp}{dt} = 0 \tag{22}$$

where

$$V_{mol} = \frac{22.4ZTp_{st}}{T_{st}p} \tag{23}$$

3. Integrated Numerical Algorithm

For the current SRPS model, the surface transmission model is solved by numerical integration method [25]. While the finite difference method is used to describe the rod string longitudinal vibration [2, 26, 27]. Since there is no fixed solution between surface and downhole model, it needs cyclic iteration to handle the whole model, which is time consuming [25]. Considering the interaction within plunger motion, fluid flow into pump and pump pressure, the improved SRPS model has a higher nonlinear degree and thus increases the difficulty of solving it. In order to reduce the solving time, the wave equation of rod string longitudinal vibration is converted into ordinary differential equations by modal superposition method. Then the surface and downhole boundary model are now in the form of ordinary differential equations at which the whole model can be solved by Runge-Kutta method directly. Besides that, solving the rod string longitudinal vibration equation is also solving the force vibration response of rod string, where (3) is converted into the following form:

$$\rho_r A_r \frac{\partial^2 u}{\partial t^2} - \rho_r E_r \frac{\partial^2 u}{\partial x^2} + \mu \frac{\partial u}{\partial t} = \rho_r A_r f(x,t) \tag{24}$$

where

$$f(x,t) = -\frac{d^2 u_a(t)}{dt^2} - \frac{\mu}{\rho_r A_r}\frac{du_a(t)}{dt} + g \tag{25}$$

And its solution can be expressed in the function of time and space by separating the variables:

$$u(x,t) = \sum_{i=1}^{\infty} \Phi_i(x)\, q_i(t) \tag{26}$$

Therefore, (24) can be expressed as

$$\begin{aligned} &\sum_{i=1}^{\infty} A_r \rho_r \Phi_i(x)\, \ddot{q}_i(t) \\ &\quad - \sum_{i=1}^{\infty} E_r A_r \frac{d^2 \Phi_i(x)}{dx^2} q_i(t) + \sum_{i=1}^{\infty} \mu \Phi_i(x)\, \dot{q}_i(t) \\ &\quad = A_r \rho_r f(x,t) \end{aligned} \tag{27}$$

Multiply the above equation by $\Phi_i(x)$, and it is integrated along the rod length. Then the following is derived:

$$\begin{aligned} &A_r \rho_r \ddot{q}_i(t) \int_0^{L_r} {\Phi_i}^2(x)\, dx \\ &\quad - E_r A_r q_i(t) \int_0^{L_r} \Phi_i(x)\, {\Phi_i}''(x)\, dx \\ &\quad + \mu \dot{q}_i(t) \int_0^{L_r} {\Phi_i}^2(x)\, dx \\ &\quad = A_r \rho_r \int_0^{L_r} \Phi_i(x)\, f(x,t)\, dx \end{aligned} \tag{28}$$

Its mode shapes and natural frequencies are

$$\begin{aligned} \Phi_i(x) &= \sqrt{\frac{2}{\rho_r A_r}} \sin\left(\frac{(2i-1)\pi}{2L_r} x\right) \\ p_{ni} &= \frac{(2i-1)\pi\sqrt{E_r/\rho_r}}{2L_r} \end{aligned} \tag{29}$$

Then (28) can be simplified as follows using mode shape orthogonality:

$$\ddot{q}_i(t) + \frac{\mu}{A_r \rho_r}\dot{q}_i(t) + \left(\frac{(2i-1)\pi}{2L_r}\right)^2 \frac{E_r}{\rho_r} q_i(t) = F_i \tag{30}$$

where

$$\begin{aligned} F_i &= \left(\frac{\mathrm{d}^2 u_a(t)}{\mathrm{d}t^2} + \mu \frac{\mathrm{d}u_a(t)}{\mathrm{d}t}\right) \frac{2\sqrt{2A_r \rho_r L_r}}{(2i-1)\pi} \\ &\quad + F_{PL}(t) \sqrt{\frac{2}{A_r \rho_r L_r}} \sin\left(\frac{(2i-1)\pi}{2}\right) \end{aligned} \tag{31}$$

Let ith-order forced vibration displacement response and velocity response be x_{i1} and x_{i2}, respectively. Then (30) can be expressed as the following form:

$$\begin{aligned}\dot{x}_{i1}(t) &= x_{i2}(t)\\ \dot{x}_{i2}(t) &= -\frac{\mu}{A_r\rho_r}x_{i2}(t) - \left(\frac{(2i-1)\pi}{2L_r}\right)^2\frac{E_r}{\rho_r}x_{i1}(t) + F_i\end{aligned} \tag{32}$$

Then suspension point load is derived.

$$\begin{aligned}F_{RL}(t) &= E_rA_r\frac{\partial u(0,t)}{\partial x} + F_r\\ &= E_rA_r\sqrt{\frac{2}{\rho_rA_rL_r}}\sum_{i=1}^{N}\frac{(2i-1)\pi}{2L_r}x_{i1}(t) + F_r\end{aligned} \tag{33}$$

The displacement and velocity of plunger are

$$\begin{aligned}u_p(t) &= u_a(t) - u(L,t)\\ &= u_a(t)\\ &\quad - \sqrt{\frac{2}{A_r\rho_rL_r}}\left(\sum_{i=1}^{i=2*j+1}x_{i1}(t) - \sum_{i=1}^{i=2*j}x_{i1}(t)\right)\\ v_p(t) &= \dot{u}_a(t) - \frac{\partial u(L,t)}{\partial t}\\ &= \dot{u}_a(t)\\ &\quad - \sqrt{\frac{2}{A_r\rho_rL_r}}\left(\sum_{i=1}^{i=2*j+1}x_{i2}(t) - \sum_{i=1}^{i=2*j}x_{i2}(t)\right)\end{aligned} \tag{34}$$

Then the integrated numerical model is given as follows:

$$\dot{\theta}_m = \omega_m$$

$$\dot{\omega}_m = \frac{1}{I_e}\left[\frac{2\lambda_kM_H\varepsilon_c\omega_n\left[\omega_n - \dot{\theta}_m\right]}{\varepsilon_c^2\omega_n^2 + \left[\omega_n - \dot{\theta}_m\right]^2} - \frac{1}{i_{bg}\eta_{bg}}\left[S_{Tf}\left(F_{RL} - F_b\right)\eta_{CL}^{k_1} - M_c\sin\left(\theta - \theta_\tau\right)\right] - \frac{1}{2}\omega_m^2\frac{dI_e}{d\theta_m}\right]$$

$$u_a(t) = \arccos\left[\frac{L_C^2 + L_K^2 - (L_R + L_P)^2}{2L_CL_K}\right] - \arccos\left(\frac{L_C^2 + L_L^2 - L_P^2}{2L_CL_L}\right)$$

$$- \arcsin\left(\frac{L_R}{L_L}\sin\left(2\pi - \theta_0 - \frac{\theta_m}{i_{bg}} + \arcsin\left(\frac{L_I}{L_K}\right)\right)\right)$$

$$x_{11}(t) = x_{12}(t)$$

$$\dot{x}_{12}(t) = -\frac{\mu}{A_r\rho_r}x_{12}(t) - \left(\frac{\pi}{2L_r}\right)^2\frac{E_r}{\rho_r}x_{11}(t) + \left(\frac{\mathrm{d}^2u_a(t)}{\mathrm{d}t^2} + \mu\frac{\mathrm{d}u_a(t)}{\mathrm{d}t}\right)\frac{2\sqrt{2A_r\rho_rL_r}}{\pi}$$

$$+ \left(A_p\left(p_d - p\right) - A_rp_d + F_f\right)\sqrt{\frac{2}{A_r\rho_rL_r}}$$

$$\dot{x}_{21}(t) = x_{22}(t)$$

$$\dot{x}_{22}(t) = -\frac{\mu}{A_r\rho_r}x_{22}(t) - \left(\frac{3\pi}{2L_r}\right)^2\frac{E_r}{\rho_r}x_{21}(t) + \left(\frac{\mathrm{d}^2u_a(t)}{\mathrm{d}t^2} + \mu\frac{\mathrm{d}u_a(t)}{\mathrm{d}t}\right)\frac{2\sqrt{2A_r\rho_rL_r}}{3\pi}$$

$$- \left(A_p\left(p_d - p\right) - A_rp_d + F_f\right)\sqrt{\frac{2}{A_r\rho_rL_r}}$$

$$\vdots$$

$$\dot{x}_{i1}(t) = x_{i2}(t)$$

$$\dot{x}_{i2}(t) = -\frac{\mu}{A_r\rho_r}x_{i2}(t) - \left(\frac{(2i-1)\pi}{2L_r}\right)^2\frac{E_r}{\rho_r}x_{i1}(t) + \left(\frac{\mathrm{d}^2u_a(t)}{\mathrm{d}t^2} + \mu\frac{\mathrm{d}u_a(t)}{\mathrm{d}t}\right)\frac{2\sqrt{2A_r\rho_rL_r}}{(2i-1)\pi}$$

$$+ \left(A_p\left(p_d - p\right) - A_rp_d + F_f\right)\sqrt{\frac{2}{A_r\rho_rL_r}}\sin\left(\frac{(2i-1)\pi}{2}\right)$$

$$F_{RL}(t) = E_r A_r \sqrt{\frac{2}{\rho_r A_r L_r}} \sum_{i=1}^{N} \frac{(2i-1)\pi}{2L_r} x_{i1}(t) + F_r$$

$$u_p(t) = u_a(t) - \sqrt{\frac{2}{A_r \rho_r L_r}} \left(\sum_{i=1}^{i=2*j+1} x_{i1}(t) - \sum_{i=1}^{i=2*j} x_{i1}(t) \right)$$

$$v_p(t) = \dot{u}_a(t) - \sqrt{\frac{2}{A_r \rho_r L_r}} \left(\sum_{i=1}^{i=2*j+1} x_{i2}(t) - \sum_{i=1}^{i=2*j} x_{i2}(t) \right)$$

*Status*1: *before opening the standing valve*

$$\frac{dp}{dt} = \frac{\left(q/\left(A_p \cdot v_p\right)\right)\left(1/\left(u_p - L_v + L_{og}\right) + \left(10^3 A_p \cdot R_J\right)/\left(N \cdot V_{mol}\right)\right) - 1/\left(u_p - L_v + L_{og}\right)}{\left[p^{-1} - 1/Z \cdot dZ/dp + 10^3 \alpha/N \cdot ZTp_{st}/T_{st}p \cdot \left(L_v + L_o - L_{og}\right)/s_p V_{mol} \cdot A_p \cdot \left(1 - \varepsilon_w\right)\right]} \cdot v_p$$

*Status*2: *after opening the standing valve*

$$\frac{dp}{dt} = \frac{\left(\left(v_f \cdot A_p + q\right)/\left(A_p \cdot v_p\right)\right)\left(1/\left(u_p - L_f - L_v + L_{og}\right) + \left(10^3 A_p \cdot R_J\right)/\left(N \cdot V_{mol}\right)\right) - 1/\left(u_p - L_f - L_v + L_{og}\right)}{\left[p^{-1} - 1/Z \cdot dZ/dp + 10^3 \alpha/N \cdot ZTp_{st}/T_{st}p \cdot \left(L_v + L_f + L_o - L_{og}\right)/s_p V_{mol} \cdot A_p \cdot \left(1 - \varepsilon_w\right)\right]}$$

$$\cdot v_p$$

*Status*3: *before opening the traveling valve*

$$\frac{dp}{dt} = \frac{\left(q/\left(A_p \cdot v_p\right)\right)\left(1/\left(u_p - L_f - L_v + L_{og}\right) + \left(10^3 A_p \cdot R_J\right)/\left(N \cdot V_{mol}\right)\right) - 1/\left(u_p - L_f - L_v + L_{og}\right)}{\left[p^{-1} - 1/Z \cdot dZ/dp + 10^3 \alpha/N \cdot ZTp_{st}/T_{st}p \cdot \left(L_v + L_f + L_o - L_{og}\right)/s_p V_{mol} \cdot A_p \cdot \left(1 - \varepsilon_w\right)\right]} \cdot v_p$$

*Status*4: *after opening the traveling valve*

$$\frac{dp}{dt} = 0$$

$$\frac{dL_f}{dt} = v_f$$

$$\frac{dv_f}{dt} = \left(L_0 - \frac{V_{og}}{A_p} + L_f + L_v \frac{A_f}{A_p}\right)^{-1} \left\{ \frac{p_s}{\rho} - \frac{p}{\rho} + \frac{v_f^2}{2} \left[\frac{A_p^2}{A_f^2} - \frac{A_p^2}{\varepsilon^2 A_f^2} - \frac{64\mu\left(L_0 - V_{og}/A_p + L_f\right)}{D^2 v_f \rho} - 1 \right] \right.$$

$$\left. - g\left(L_0 - \frac{V_{og}}{A_p} + L_f + L_v\right) \right. \tag{35}$$

4. Optimization Model

4.1. Optimization Goal. As mostly developed oil-field moves into the mid and late stage and the OWD begins to decline gradually, energy-saving, production-increasing, and reducing load variation as much as possible are particularly important. Then we take pump fullness e_{pf}, suspension point load amplitude F_{RLA}, crank torque standard deviation M_{csd}, and motor input power average $\overline{P}_m$ as the optimization goal to build a multitarget model. Suspension point load and crank torque can be solved directly by (35). The motor input power and pump fullness calculation formula are deduced as follows:

$$P_m = M_{ed}\dot{\theta}_m + P_0 + \left[\left(\frac{1}{\eta_H} - 1\right)P_H - P_0\right]\left(\frac{M_{ed}\dot{\theta}_m}{P_H}\right)^2 \tag{36}$$

$$e_{pf} = \frac{L_f - \int_0^{t_u} q\,dt - \left(L_o - L_{og}\right)}{u_{pu}} \tag{37}$$

where P_0 is the no-load power of motor, kW; P_H is the motor rated power, kW; η_H is the motor rated efficiency, kW; u_{pu} is the plunger displacement when it is arriving at dead top center.

So the objective function is

$$\Omega\left(e_{pf}(\mathbf{X}), F_{RLA}(\mathbf{X}), M_{csd}(\mathbf{X}), \overline{P}_m(\mathbf{X})\right) = K_1 e_{pf}(\mathbf{X}) + K_2 F_{RLA}(\mathbf{X}) + K_3 M_{csd}(\mathbf{X}) + K_4 \overline{P}_m(\mathbf{X}) \quad (38)$$

where K_1, K_2, K_3, and K_4 are the weight coefficients.

4.2. Design Variables. The objective function can be expressed as the function of the swabbing parameters when the SRPS type and oil well basic parameters are confirmed. In this paper, the swabbing parameters denote stroke S, stroke frequency n_s, pump diameter D_d, pump depth L_{pd}, crank balance radius r_c, and rod string combination (the jth rod string diameter and length are d_j and L_j, respectively, $k = 1, 2, \ldots, m$). Then the design variables are shown as follows:

$$\mathbf{X} = \left\{S, n_s, D_d, L_{pd}, \left(d_j, L_j; j = 1, 2, \cdots m\right)\right\} \quad (39)$$

4.3. Constraints

(a) Crank Balance Degree. Crank balance degree indicates the load fluctuation to a certain degree and it needs to be kept at a high value:

$$0.95 \le \frac{M_{cku}}{M_{ckd}} \le 1 \quad (40)$$

where M_{cku} and M_{ckd} are the maximum crank torque when plunger is at upstroke and downstroke, respectively, N·m.

(b) Ground Device Carrying Capacity. The suspension point load, crank torque and motor torque, at any time $[0, T]$ do not go beyond the allowable range $\{\max(F_{RL}), \min(F_{RL}); \max(M_c), \min(M_c); \max(M_{ed}), \min(M_{ed})\}$ for the given type:

$$\begin{aligned} \min\left(F_{RL}\right) \le F_{RL} \le \max\left(F_{RL}\right) \\ \min\left(M_{ck}\right) \le M_{ck} \le \max\left(M_{ck}\right) \\ \min\left(M_{ed}\right) \le M_{ed} \le \max\left(M_{ed}\right) \end{aligned} \quad (41)$$

(c) Rod String Strength. The maximum and minimum stress of any point x along the rod string does not exceed permissible stress range in one cycle:

$$[\sigma_{\min}] \le \sigma_{rs} \le [\sigma_{\max}] \quad (42)$$

(d) Swabbing Parameters. Each oil well has different limit on the swabbing parameters in accordance with the device type and actual operation; hence their allowable variation ranges are adjustable.

Figure 8: Dynamometer sensor.

4.4. Optimization Algorithm. In summary, this multivariable optimization model is established with nonlinear restriction and nonlinear objective function. So as to seek the best results, the genetic algorithm is applied to solve it.

5. Test and Verification

Surface dynamometer card is a closed graph recording polished rod loads versus rod displacement over a SRPS cycle, which is generally collected and taken as an index to estimate the operation of SRPS. In this paper, based on the dynamometer sensor shown in Figure 8, four test wells are used to validate the improved SRPS model. The oil well parameters are listed in Table 1, and the simulation and field test results are given in Figure 9. According to the plotted curves, the simulation results are basically consistent with that in measured, and the improved SRPS model is accurate enough to be proposed for engineering practices.

6. Dynamic Response Comparison

Pump dynamometer card is a closed graph recording plunger loads versus plunger displacement over a SRPS cycle. It is determined by multifactors such as stroke, stroke frequency, pump diameter, pump depth, dynamic liquid level, and the other oil well parameters. The difference between the current SRPS model and the improved SRPS model proposed in this paper is whether to consider the PFFP. In view of this, the oil operating status is divided into two forms as follows: (1) the fluid always keeps pace with the plunger when it is being sucked into the pump; (2) the fluid is unable to follow with the plunger. Then two oil wells are selected: well#1 with sufficient OWD and well#2 with insufficient OWD. Figure 10 describes the plunger and fluid velocity during upstroke based on the improved SRPS model. It can be concluded that when the well has sufficient OWD and the fluid possesses good ability of keeping pace with the plunger; when the well has insufficient OWD, the fluid velocity lags behind the one of plunger at the beginning, whereas it is

Table 1: Oil well basic parameters.

Well	#1	#2	#3	#4
Motor type	YD280S-8	Y250M-6	Y250M-6	YD280S-6
Pumping unit type	CYJ10-3-53HB	CYJ10-3-53HB	CYJ10-3-53HB	CYJ10-3-53HB
Stroke length (m)	3	3	3	3
Stroke frequency (min^{-1})	3.5	3	4	6
Pump diameter (mm)	57	44	38	44
Pump clearance level	1	2	2	1
Pump depth (m)	890	1377	1138	1430
Sucker-rod string (mm × m)	25∗890	19∗673+22∗704	19∗672+22∗466	19∗720+22∗710
middle depth of reservoir (m)	1000	1492	1569	1600
Crude oil density (kg/m^3)	795	857	857	850
Water content (%)	95	97	92	98
Dynamic liquid level (m)	880	1347	757	1340
Casing pressure (Pa)	0.2	0.3	0.3	0.2
Oil pressure (Pa)	0.3	0.3	0.3	0.2
Fluid dynamic viscosity (Pa·s)	0.006	0.007	0.007	0.006
Gas oil ratio (m^3/m^3)	20	19	40	80
Plunger length (m)	1.2	1.2	1.2	1.2
Clearance length (m)	0.5	0.5	0.5	0.5

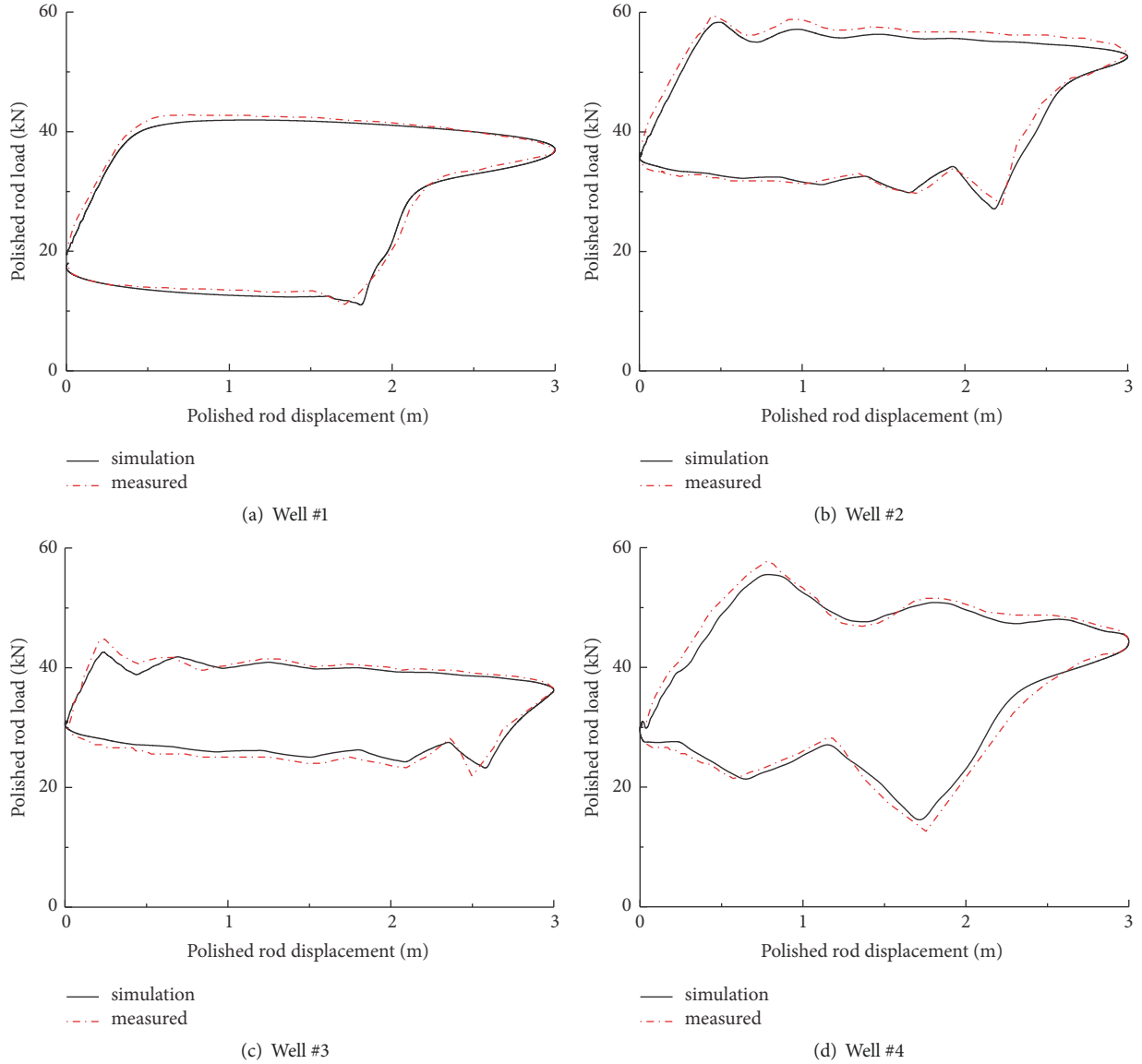

Figure 9: Suspension point dynamometer card comparison between the simulated and measured.

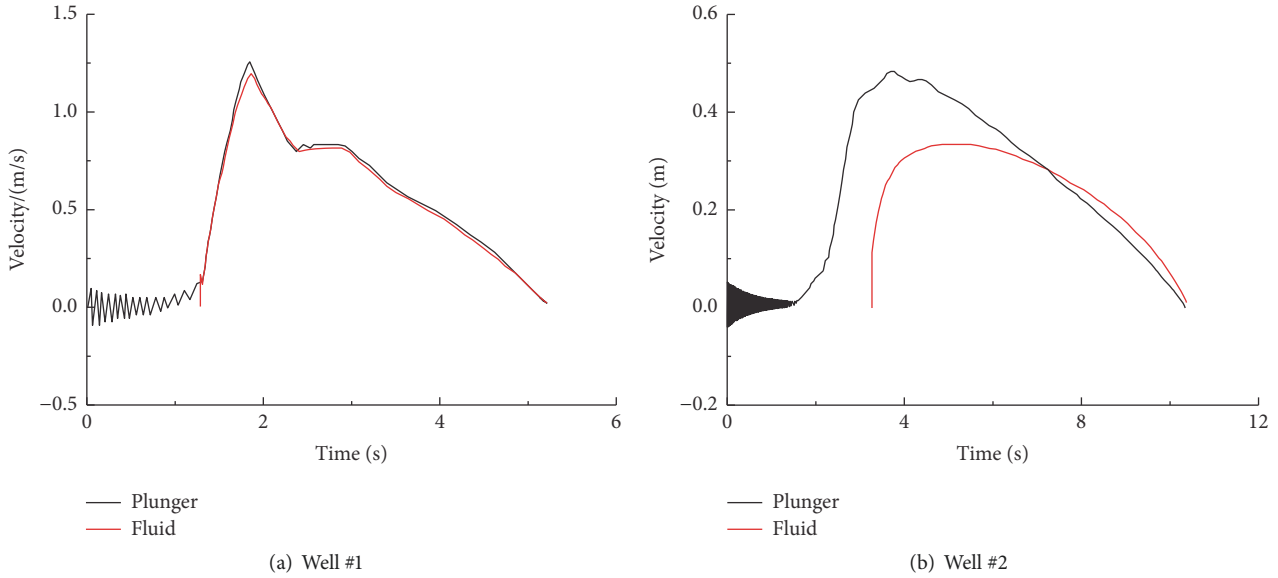

(a) Well #1 (b) Well #2

Figure 10: Plunger and fluid velocity.

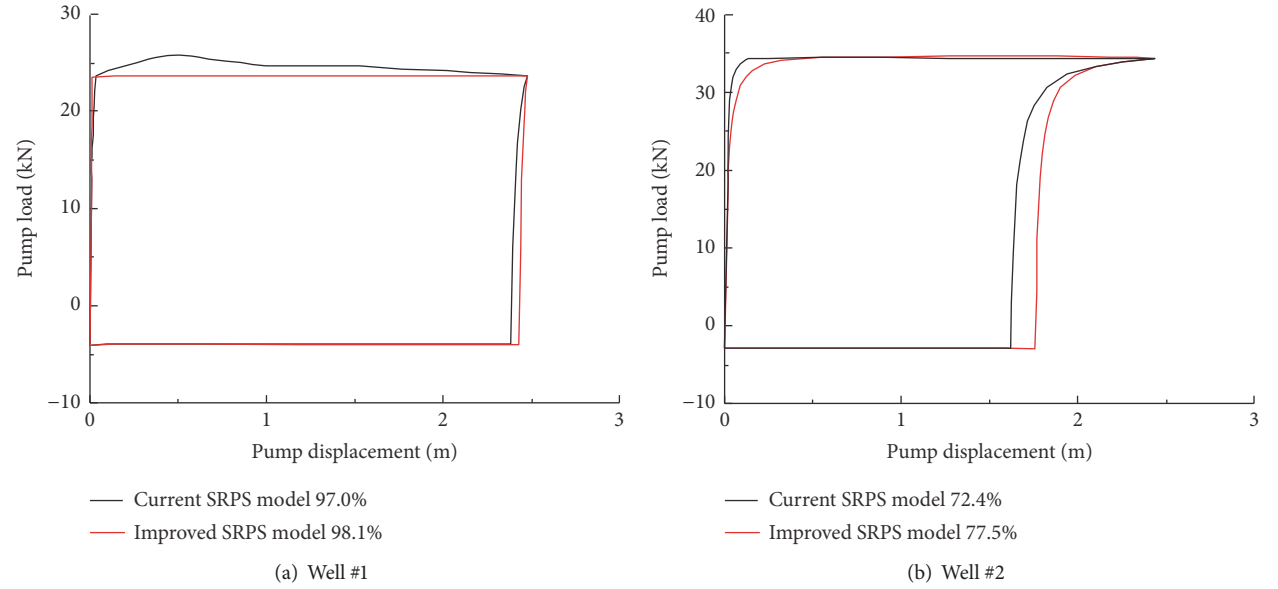

(a) Well #1 (b) Well #2

Figure 11: Comparison of pump dynamometer card.

faster after a certain time period. Then the comparisons of pump dynamometer card are executed by the two models; meanwhile their individual pump fullness result is given at the end of the legend (Figure 11).

Pump dynamometer card is very important method and normally used to diagnose the pump operations, particularly whose shape is more similar to a rectangle, the pump is closer to the fullness [28]. Hence, from Figure 11, it can be known that the pump fullness of current SRPS model is higher than that of the improved one depending on the qualitative judgment, and this conclusion is consistent with the quantitative calculation result, meanwhile this gap for the well #2 is bigger than well #1. According the above description, we can know that the pump fullness calculation result is on the high side if the PFFP is not considered, and this phenomenon will become more obvious for the well with insufficient OWD.

The load presented by the left, upper, right, and lower borderline of pump dynamometer card is the results of pump moving from phase 1 to 4 in turn. Therefore, its upper borderline describes the pump load when fluid is pumped into the barrel. From Figure 11(a), it can be found that the upper borderline load simulated by the improved SRPS model is significantly larger than the one of current. For Figure 11(b), this difference can be neglected. Based on (1) and (2), the pump pressure keeps constant as p_s when fluid is

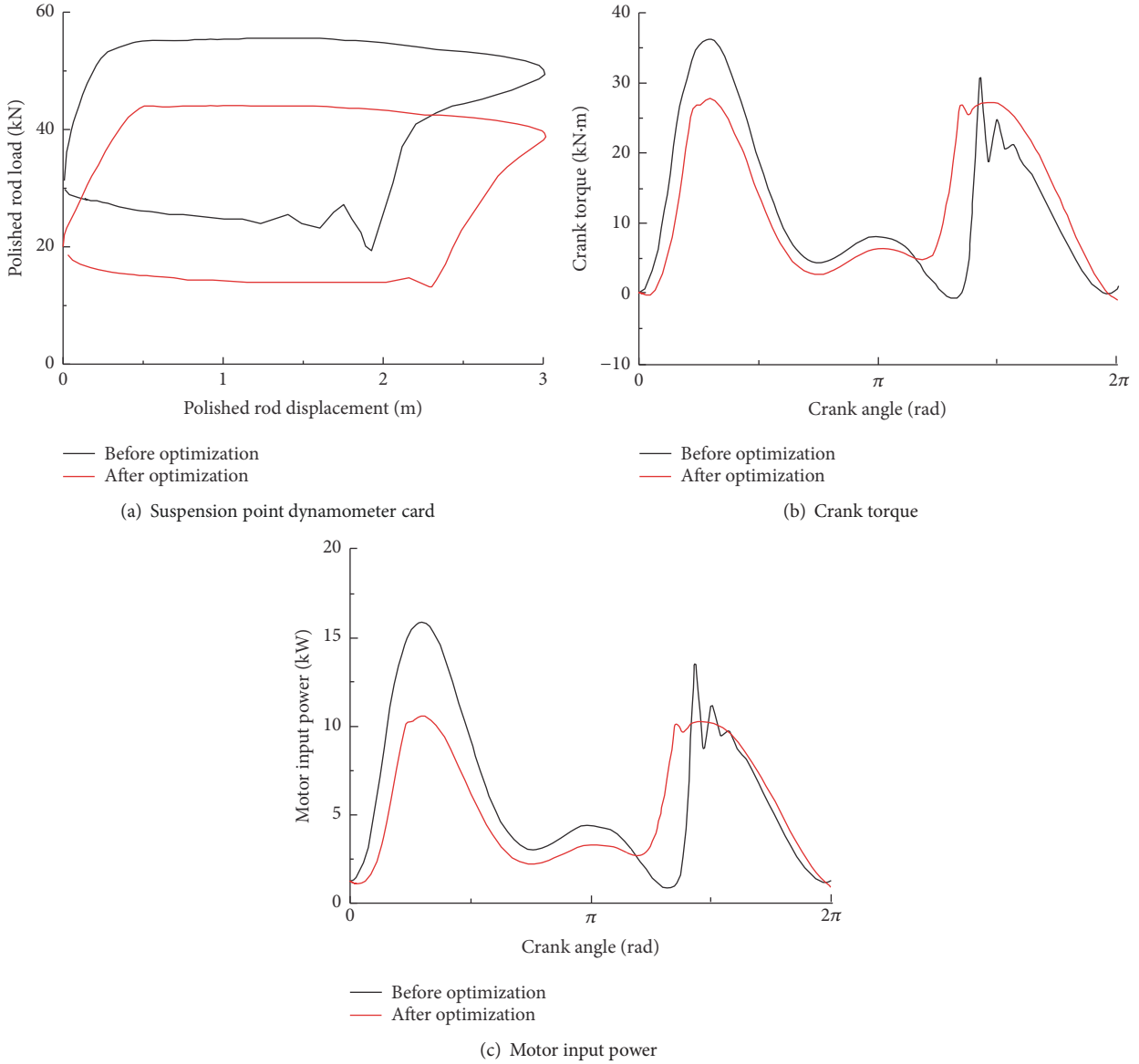

Figure 12: Dynamic response comparison before and after optimization.

sucked into the pump and then the corresponding pump load is a fixed value. Due to the new model takes into account of PFFP, a pressure drop will be brought, which will vary with the fluid velocity. Combined with (1), this pressure drop will lead to the pump load increases. Figure 10 shows that the fluid velocity of well #1 is larger than that of well #2, and this is the reason why the difference of upper borderline load between the two models is obvious. This illustrates the error on the upper borderline load of pump dynamometer card depending on the velocity at which the fluid flows into the pump.

7. Optimization Test

Based on the above models, a simulation and optimization software is developed by MATLAB. One well with insufficient OWD is tested. Its original swabbing parameters are as follows: stroke S is 3 m, stroke frequency n_s is 3 min^{-1}, pump diameter D_d is 57mm, pump depth L_{pd} is 900 m, crank balance radius r_c is 1.2 m, and rod string combination $d_j \times L_j$ is 25 mm × 524 m+22 mm × 376 m. And its swabbing parameters after optimizing are as follows stroke S is 3 m, stroke frequency n_s is 2.5 min^{-1}, pump diameter D_d is 57mm, pump depth L_{pd} is 990 m, crank balance radius r_c is 0.9 m, and rod string combination $d_j \times L_j$ is 22 mm × 426 m+19 mm × 564 m. The comparisons before and after optimization are shown in Figure 12 and Table 2.

From the above comparison results, some conclusions are obtained:

(1) After optimization, the maximum and minimum of suspension point load are all decreased, and the load

Table 2: Specific parameters comparison before and after optimization.

	Suspension point load			Crank torque		Motor input power			Pump fullness
	Maximum	Minimum	Amplitude	Standard deviation	Balance degree	Maximum	Minimum	mean	
Before optimization	55.5 kN	19.0 kN	36.5 kN	10.7 kN	85.4 %	15.9 kW	0.9 kW	6.2 kW	72.5 %
After optimization	44.1 kN	13.2 kN	30.9 kN	9.4 kN	97.8 %	10.6 kW	1.0 kW	5.4 kW	90.8 %
	↓ 20.5 %	↓ 30.5 %	↓ 15.3 %	↓ 12.1 %	↑ 14.5 %	↓ 33.3 %	↑ 11.1 %	↓ 12.9 %	↑ 25.2 %

amplitude is lowered by 15.3 %. It can contribute to enhance the rod string life and prolong the maintenance period.

(2) After optimization, the standard deviation of crank torque is reduced by 12.1 %, and its balance degree is raised by 14.5 %. It illustrates that the load torque fluctuation is cut down, which can minimize damage to transmission parts and improve the motor efficiency.

(3) After optimization, the pump fullness is improved by 25.2 %. It is conducive to improve pump efficiency and production.

(4) After optimization, it plays a role of peak shaving and valley filling for motor input power and extends the operational life, meanwhile power saving rate is 12.9 %.

8. Conclusions

(1) In this article, an improved SRPS model is presented, considering the couple effect of pumping fluid and plunger motion on the dynamic response of SRPS, instead of the existing models that assume the pumping fluid volume is always equal to plunger travelling volume. The Runge-Kutta method is applied to solve the whole system model trough transforming the rod string longitudinal vibration equation into ordinary differential equations. And the SRPS model's precision has been validated by adopting surface dynamometer card.

(2) Two oil wells are served to compare the difference between the current SRPS model and the improved one. The results indicate that the current SRPS model is relatively low in calculating pump fullness, and this gap will increase with the reduction of OWD; the influence of fluid flowing into the pump on pump load cannot be ignored when the fluid velocity is high. Therefore, the PFFP is necessary to be considered in order to improve the simulation accuracy.

(3) On the basis of the improved SRPS model, a multitarget optimization model is proposed in purpose of improving production, decreasing load fluctuation and saving energy. By comparison, the optimal scheme can achieve the decreasing of maximum and minimum suspension point load, crank torque fluctuation and energy consumption, as well as improving the system balance degree and pump fullness. In summary, it improves the dynamic behavior of SRPS.

Data Availability

The data used to support the findings of this study are available from the corresponding author upon request.

Conflicts of Interest

The authors declare that they have no conflicts of interest.

Acknowledgments

National Natural Science Foundation of China (Grant no. 51174175), China Scholarship Council (Grant no. 201708130108), Hebei Natural Science Foundation (Grant no. E201703101) are acknowledged.

References

[1] T. A. Aliev, A. H. Rzayev, G. A. Guluyev, T. A. Alizada, and N. E. Rzayeva, "Robust technology and system for management of sucker rod pumping units in oil wells," *Mechanical Systems and Signal Processing*, vol. 99, pp. 47–56, 2018.

[2] S. Gibbs, "Predicting the Behavior of Sucker-Rod Pumping Systems," *Journal of Petroleum Technology*, vol. 15, no. 07, pp. 769–778, 1963.

[3] D. R. Doty and Z. Schmidt, "Improved model for sucker rod pumping," *SPE Journal*, vol. 23, no. 1, pp. 33–41, 1983.

[4] I. N. Shardakov and I. N. Wasserman, "Numerical modelling of longitudinal vibrations of a sucker rod string," *Journal of Sound and Vibration*, vol. 329, no. 3, pp. 317–327, 2010.

[5] S. G. Gibbs, "Computing gearbox torque and motor loading for beam pumping units with consideration of inertia effects," *SPE J*, vol. 27, pp. 1153–1159, 1975.

[6] J. Svinos, "Exact Kinematic Analysis of Pumping Units," in *Proceedings of the SPE Annual Technical Conference and Exhibition*, San Francisco, California, 1983.

[7] D. Schafer and J. Jennings, "An Investigation of Analytical and Numerical Sucker Rod Pumping Mathematical Models," in *Proceedings of the SPE Annual Technical Conference and Exhibition*, pp. 27–30, Dallas, Texas, 1987.

[8] G. Takács, *Sucker-Rod Pumping Manual*, Pennwell Books, Tulsa, 2003.

[9] G. W. Wang, S. S. Rahman, and G. Y. Yang, "An improved model for the sucker rod pumping system," in *Proceedings of the 11th Australasian Fluid Mechanics Conference*, pp. 14–18, Hobart, Australia, December 1992.

[10] S. D. L. Lekia and R. D. Evans, "A coupled rod and fluid dynamic model for predicting the behavior of sucker-rod pumping systems," *SPE Production & Facilities*, vol. 10, no. 1, pp. 26–33, 1995.

[11] J. Lea and P. Pattillo, "Interpretation of Calculated Forces on Sucker Rods," *SPE Production & Facilities*, vol. 10, no. 01, pp. 41–45, 1995.

[12] P. A. Lollback, G. Y. Wang, and S. S. Rahman, "An alternative approach to the analysis of sucker-rod dynamics in vertical and deviated wells," *Journal of Petroleum Science and Engineering*, vol. 17, no. 3-4, pp. 313–320, 1997.

[13] L. Guo-hua, H. Shun-li, Y. Zhi et al., "A prediction model for a new deep-rod pumping system," *Journal of Petroleum Science and Engineering*, vol. 80, no. 1, pp. 75–80, 2011.

[14] L.-M. Lao and H. Zhou, "Application and effect of buoyancy on sucker rod string dynamics," *Journal of Petroleum Science and Engineering*, vol. 146, pp. 264–271, 2016.

[15] O. Becerra, J. Gamboa, and F. Kenyery, "Modelling a Double Piston Pump," in *Proceedings of the SPE International Thermal Operations and Heavy Oil Symposium and International Horizontal Well Technology Conference*, Calgary, Alberta, Canada, 2002.

[16] A. L. Podio, J. Gomez, A. J. Mansure et al., "Laboratory instrumented sucker-rod pump," *J. Pet. Technol*, vol. 53, no. 05, pp. 104–113, 2003.

[17] Z. H. Gu, H. Q. Peng, and H. Y. Geng, "Analysis and measurement of gas effect on pumping efficiency," *China Petroleum Machinery*, vol. 34, no. 02, pp. 64–69, 2006.

[18] M. Xing, "Response analysis of longitudinal vibration of sucker rod string considering rod buckling," *Advances in Engineering Software*, vol. 99, pp. 49–58, 2016.

[19] S. Miska, A. Sharaki, and J. M. Rajtar, "A simple model for computer-aided optimization and design of sucker-rod pumping systems," *Journal of Petroleum Science and Engineering*, vol. 17, no. 3-4, pp. 303–312, 1997.

[20] L. S. Firu, T. Chelu, and C. Militaru-Petre, "A modern approach to the optimum design of sucker-rod pumping system," in *SPE Annual Technical Conference and Exhibition*, pp. 1–9, Denver, Colorado, 2003.

[21] X. F. Liu and Y. G. Qi, "A modern approach to the selection of sucker rod pumping systems in CBM wells," *Journal of Petroleum Science and Engineering*, vol. 76, no. 3-4, pp. 100–108, 2011.

[22] S. M. Dong, N. N. Feng, and Z. J. Ma, "Simulating maximum of system efficiency of rod pumping wells," *Journal of System Simulation*, vol. 20, no. 13, pp. 3533–3537, 2008.

[23] M. Xing and S. Dong, "A New Simulation Model for a Beam-Pumping System Applied in Energy Saving and Resource-Consumption Reduction," *SPE Production & Operations*, vol. 30, no. 02, pp. 130–140, 2015.

[24] Y. X. Wu, Y. Li, and H. Liu, *Electric Motor and Driving*, Chemical Industry Press, Beijing, 2008.

[25] S. M. Dong, *Computer Simulation of Dynamic Parameters of Rod Pumping System Optimization*, Petroleum Industry Press, Beijing, Chinese, 2003.

[26] F. Yavuz, J. F. Lea, J. C. Cox et al., "Wave equation simulation of fluid pound and gas interference," in *Proceedings of the SPE Production Operations Symposium*, pp. 16–19, Oklahoma City, Oklahoma, April 2005.

[27] D. Y. Wang and H. Z. Liu, "Dynamic modeling and analysis of sucker rod pumping system in a directional well, Mechanism and Machine Science," in *Proceedings of the ASIAN MMS 2016 & CCMMS*, pp. 1115–1127, 2017.

[28] F. M. A. Barreto, M. Tygel, A. F. Rocha, and C. K. Morooka, "Automatic downhole card generation and classification," in *Proceedings of the SPE Annual Technical Conference*, pp. 6–9, Denver, Colorado, 1996.